STRENGTH AND CONTACT DAMAGE RESPONSES IN A SODA-LIME-SILICATE AND A BOROSILICATE GLASS

A. A. Wereszczak,* K. E. Johanns, and T. P. Kirkland
Oak Ridge National Laboratory
Oak Ridge, TN 37831-6068

C. E. Anderson, Jr.
Southwest Research Institute
San Antonio, TX 78228

T. Behner
Fraunhofer Institut fur Kurzzeitdynamik
Ernst-Mach Institut, Frieburg, Germany

P. Patel
U. S. Army Research Laboratory
Aberdeen Proving Ground, MD 21005

D. W. Templeton
U. S. Army RDECOM-TACOM
Warren, MI 48397

ABSTRACT

Although soda-lime-silicate glass is typically used as windows in ground vehicles, borosilicate glass is an interesting alternative because its density is about 10% less and therefore its use could reduce vehicle weight. The US Army RDECOM is characterizing both glasses in a variety of ways to compare their performances and judge if the use of borosilicate glass is a worthy substitute. This study supported that through a series of quasi-static strength and spherical (Hertzian) indentation tests. Their results were then combined to construct "Damage/Design Maps" which are advocated here to help guide the use of these glasses in ground vehicles. If static strength and indentation responses are translatable to ballistic performance, then this study shows improved ballistic performance of "float-glasses" can be achieved through appropriate selection of glass based on the thickness and the appropriate orientations of their "air" and "tin" sides.

1. INTRODUCTION

Windshield and side windows in Army ground vehicles are a huge consumer of glass. The glass must provide multi-hit protection, must be large enough so not to impede the driver's field of view, and have a desirably low weight (Sands et al., 2004). Regarding the latter sought attribute, borosilicate glass is an interesting alternative to conventionally used soda-lime-silicate glasses for windows because its density is approximately 10% less and therefore its use could reduce vehicle weight.

The US Army RDECOM is characterizing both glasses in a variety of ways to compare the performances and judge if borosilicate glass is a worthy substitute. Most of the testing and modeling involves high rate ballistics analyses of the two glasses. In parallel to that, interest exists to probe the relevance and usefulness of quasi-static mechanical testing because it is inherently less expensive than ballistic evaluations and simpler to conduct. If the results from quasi-static testing could ultimately be translated to predicted ballistic response, then such testing could be used to screen candidate armor materials, and enable ballisticians to confidently devote their energies to the characterization and modeling of the better grades.

The quasi-static testing of a soda-lime-silicate glass and a borosilicate glass was pursued in this study through equibiaxial flexure strength and static spherical (or Hertzian) indentation. Knowledge of flexure strength is pertinent because it, with the elastic properties, can be used to estimate how much deflection glass can sustain without fracturing. If glasses have different strengths and elastic properties (which these two exhibited), then their deflection will be different against the same applied force. Hertzian indentation is also useful because it can generate many of the same damage mechanisms that occur during a ballistic event. Such indentation can enable the study of contact-damage-responses in candidate materials, assessment of energy-absorbing capability, and ideally, the estimation of dwell response.

Design/damage maps can be constructed with the generated flexure and indentation data. They are useful because they portray the competition of the system response to various factors such as the glass thickness and how the glass is supported. For example, if the system is not stiff or thick enough, then a material's contact resistance properties cannot be exploited because the material fractures before those energy-absorbing mechanisms ever become operable. Conversely, if the system is too thick, then there is an unnecessary excess of material (i.e., weight) associated with the desirable exploitation of those contact-damage-mechanisms. The objective is to identify the optimal compromise that results in the energy-absorbing mechanisms being fully exploited with minimum weight. That objective can be satisfied through the strength and indentation testings that were conducted in this study.

Report Documentation Page

Form Approved
OMB No. 0704-0188

1. REPORT DATE	2. REPORT TYPE	3. DATES COVERED
01 NOV 2006	**N/A**	**-**

4. TITLE AND SUBTITLE	5a. CONTRACT NUMBER
Strength And Contact Damage Responses In A Soda-Lime-Silicate And A Borosilicate Glass	5b. GRANT NUMBER
	5c. PROGRAM ELEMENT NUMBER
6. AUTHOR(S)	5d. PROJECT NUMBER
	5e. TASK NUMBER
	5f. WORK UNIT NUMBER
7. PERFORMING ORGANIZATION NAME(S) AND ADDRESS(ES) **Oak Ridge National Laboratory Oak Ridge, TN 37831-6068**	8. PERFORMING ORGANIZATION REPORT NUMBER
9. SPONSORING/MONITORING AGENCY NAME(S) AND ADDRESS(ES)	10. SPONSOR/MONITOR'S ACRONYM(S)
	11. SPONSOR/MONITOR'S REPORT NUMBER(S)

12. DISTRIBUTION/AVAILABILITY STATEMENT
Approved for public release, distribution unlimited

13. SUPPLEMENTARY NOTES
See also ADM002075., The original document contains color images.

14. ABSTRACT

15. SUBJECT TERMS

16. SECURITY CLASSIFICATION OF:			17. LIMITATION OF ABSTRACT	18. NUMBER OF PAGES	19a. NAME OF RESPONSIBLE PERSON
a. REPORT	b. ABSTRACT	c. THIS PAGE			
unclassified	**unclassified**	**unclassified**	**UU**	**8**	

Standard Form 298 (Rev. 8-98)
Prescribed by ANSI Std Z39-18

2. EXPERIMENT

2.1 Description of Materials

Two glasses were evaluated in this study. Starphire® (PPG, Pittsburgh, PA) is a soda-lime-silicate with a density of 2.49 g/cm^3. Borofloat® (Schott North America, Louisville, KY) is a borosilicate with a density of 2.22 g/cm^3. Disks of both glasses, having a nominal diameter of 100 mm and a thickness of 3.2 mm, were used in all the mechanical testing. Elastic properties were measured through the combined use of resonant ultrasound spectroscopy and modal analysis using a method described elsewhere (Wereszczak, 2006b; Wereszczak, 2006c). The Young's Modulus and Poisson's ratio of Starphire® was 73.1 GPa and 0.203, respectively, and 63.1 GPa and 0.180 for Borofloat®.

Both glasses were processed through a "float-glass" process. The molten glass is poured onto a molten bath of tin, and because glass has a lower specific gravity, it floats and enables the ultimate formation of large flat sheets of glass. Because of this processing method, this study's investigators wanted to explore if there was a "side" dependence on properties; namely, are the properties of the "tin" (surface of the glass in contact with the molten tin) and "air" (surface exposed to the furnace air) sides different. As a consequence of this, there were a total of four conditions in this study: Starphire-air, Starphire-tin, Borofloat-air, and Borofloat-tin.

2.2 Mechanical Testing

Ring-on-ring, or equibiaxial, flexure testing was used to measure and compare strengths of the four conditions. Sixteen to eighteen specimens were tested per condition. A schematic of the setup is shown in Fig. 1. Testing adhered to ASTM practices for this test type (ASTM C1499, 2005a). Upper and lower ring diameters of 25 and 75 mm, respectively, were used. A semi-articulated fixture was used to minimize any misaligned loading. Graphite foil was used in all tests to lessen stress concentrations between the specimens and upper and lower rings. Testing was done in displacement control at a rate of 0.5 mm/min and failure load was recorded. This rate was deemed rapid enough to avoid slow crack growth effects (Pavelchek and Doremus, 1976). Failure stress was calculated using the appropriate expression in ASTM C1499. Two parameter Weibull distributions were determined following ASTM practice (ASTM C1239, 2005b).

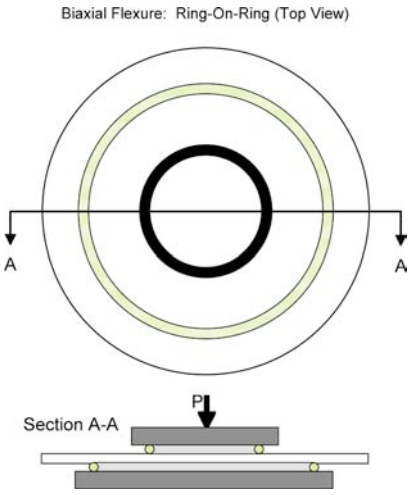

Figure 1. Schematic of the ring-on-ring equibiaxial flexure strength test setup.

There are a variety of crack types that can occur during spherical indentation of glass, and the primary types are illustrated in Fig. 2. There is a huge amount of literature on these mechanisms in glass, including the sequence for formation, for glass (e.g., Tillet, 1956; Swain and Hagen, 1976; Cook and Pharr, 1990; Lardner et al., 1997; and Lawn, 1998).

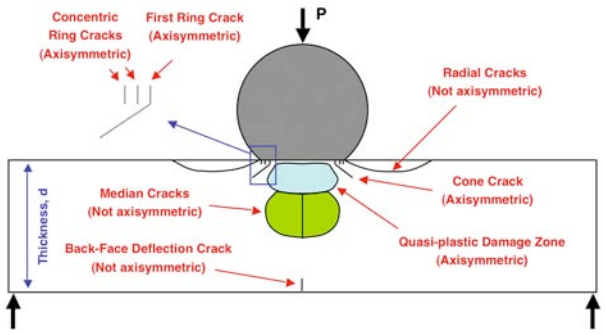

Figure 2. Schematic of the crack and damage mechanisms that can be operative during spherical indentation of a glass plate that can deflect. This can also be viewed as an indentation-ball-on-ring test.

Two different methods of spherical indentation tests were conducted to sample the effects of the damage mechanisms.

Ring cracking is the first crack type to form, so one test method focused on identifying the force to initiate it; it essentially determines the loading condition when Hertzian damage starts. A schematic of the test setup used to measure this is shown in Fig. 3. A spherical 500-µm-diameter diamond indenter was used for these tests. The indenter was loaded at a compressive displacement rate of 1 µm/s until the acoustic emission signal

registered an event. The validity of this was checked with numerous tests through ring crack examination via optical microscopy. The event's associated load was identified as the ring-crack load.

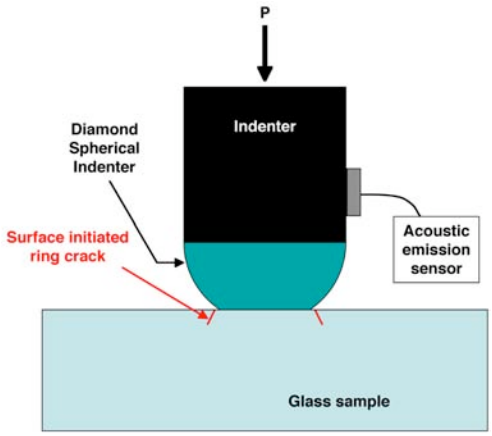

Figure 3. Side view schematic of the spherical indentation setup used to measure the ring-crack initiation load.

The second indentation method used measured the indenter force and indenter depth of penetration during a loading and unloading (triangular) waveform. The system has been described elsewhere (Wereszczak and Johanns, 2006a). A schematic of this method is shown in Fig. 4. If the material responds elastically, then a plot of indenter force as a function of indenter depth of penetration will show no hysteresis between the loading and unloading portions. However, when the material responds inelastically, then hysteresis is formed and it can be used to interpret the energy absorption associated with the operative damage mechanisms illustrated in Fig. 2. A spherical 300-µm-diameter diamond indenter was used for these tests. The indenter was loaded at a compressive displacement rate of 1 µm/s up to some desired maximum load and then unloaded. Because of the use of this smaller diameter indenter, the produced stresses can be quite large for modest applied loads. These high stresses were effective at producing most of the mechanisms shown in Fig. 2. Lastly, this second method enabled us to make some very preliminary comparisons of high-stress material response from quasi-static and ballistic testing.

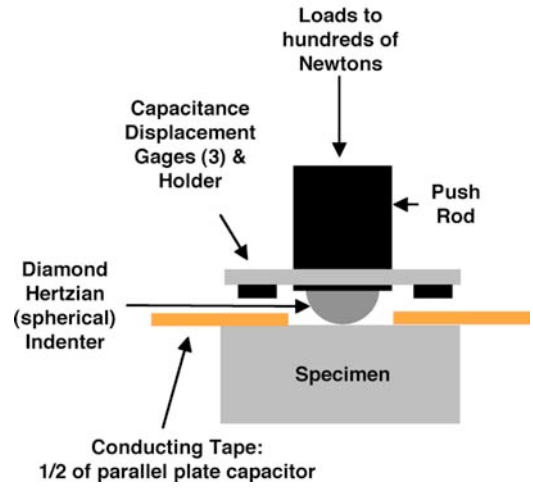

Figure 4. Side view schematic of the spherical indentation setup used to measure indent depth of penetration.

2.3 Design/Damage Maps

The desire to construct maps that combine strength and indentation responses have been in existence for several years (Lardner et al., 1997; Rhee et al., 2001). The relationship between force and fracture from bending (see "back-face deflection crack in Fig. 2) as a function of tile thickness has a d^2 dependency as shown in Fig. 5(a). Though elastic properties and flexure strength affect this relationship, a geometrical parameter (thickness) does too, thus making this a system response. If the specimen is "semi-infinitely thick", then applying an indentation force causes contact-induced damage as shown in Fig. 2, and a series of crack types can be produced with increasing applied loads (Fig. 5(b)). This is a material response because deflection-induced stresses are not a significant contributor to the damage.

The contributions and competition of damage from deflection and contact can then finally be portrayed by a Design/Damage Map - see Fig. 5(c). The construction of such a map for the four test conditions in this study was sought. Equibiaxial flexure strength testing would produce information on the system response while ring-crack testing would provide a measure of material response (i.e., contact-damage-resistance).

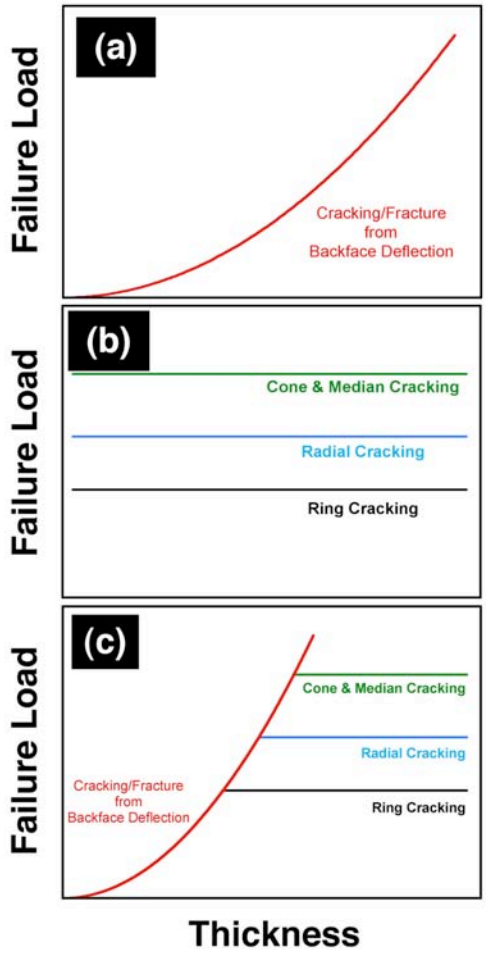

Figure 5. Failure load as a function of deflection (a) and indentation loads to initiate different mechanisms (b) can be combined (c) to generate a "Design/Damage Map."

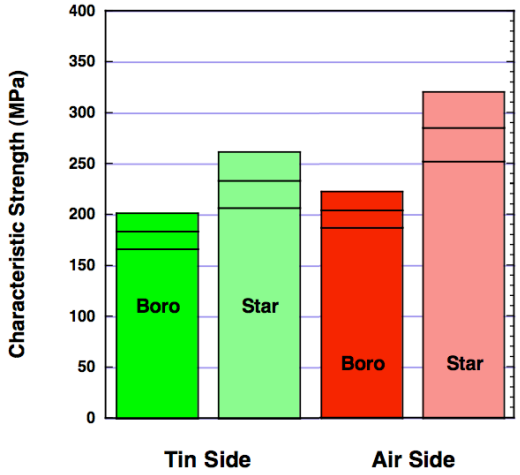

Figure 6. Characteristic strength comparison as a function of glass material and test side. The middle horizontal line on each bar is the strength and those above and below it are ± 95% confidence intervals.

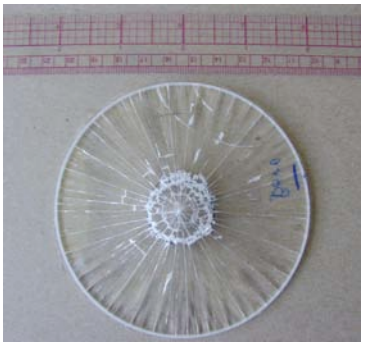

Figure 7. Example of a fractured glass disk tested in ring-on-ring equibiaxial flexure.

3. RESULTS AND DISCUSSION

3.1 Equibiaxial Flexure Strength

The flexure strength of Starphire® was greater than that of Borofloat®, and the air side of both was stronger than their tin side. Fig. 6 illustrates this comparison. For the same thickness of glass, this means that the Starphire® can withstand larger flexure loads than the Borofloat®, and both glasses can withstand higher flexure loads if their tin sides are oriented to be the impact side (i.e., the air side being the back face side).

All the specimens exhibited a "spoke-like" fracture pattern. A representative fracture pattern in shown in Fig. 7. The fracture initiated on the tensile surface of the flexure specimen and very close to the center of the gage section. The initiation of all fractures occurred within that gage section (where the equibiaxial stress is constant throughout).

3.2 Indentation Response

The trends were reversed for critical loads that initiated ring cracking. As illustrated in Fig. 8, the Borofloat® glass was able to withstand higher, damage-free contact forces than the Starphire® glass and the tin side of both glasses could withstand higher, damage-free contact forces than their air sides. *These trends of flexure strength and indentation responses are synergistic if the tin and air sides are oriented to be the contact and back-face sides, respectively.*

The progression of contact damage with increasing indentation load is illustrated in Fig. 9. A ring crack forms first. Additionally loading causes concentric ring cracks to form followed by the initiation of radial cracks. Cone cracking then is initiated and then median cracking. Median cracking is easily discernable from radial cracking in glasses through simple focus adjustments

made with an optical microscope. Referring to Figs. 2 and 9, radial cracks will appear in focus on the surface while median cracks will not be because they form in the bulk.

The indenter senses compliance increases differently for the various crack types that form. Referring to both Figs. 9-10, the indenter does not detect a significant amount of compliance increase with the formation of the initial ring crack (22 N) or the concentric ring cracks that soon follow. This is because the ring crack forms just outside the indenter's contact area, so the indenter senses the material is still responding elastically although damage has obviously initiated. The indenter senses compliance increase with the initiation of radial cracking (31 N) and cone cracking (40 N) and there is a further compliance rate increase with the formation of median cracking (53 N).

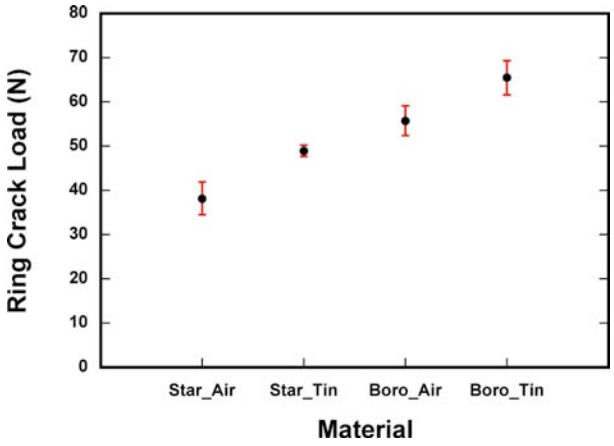

Figure 8. Comparison of ring crack loads for the four combinations. For example, indentation of the air side of the Starphire® is labeled as "Star_Air."

3.3 Ballistic Link to Indentation Damage?

Does the initiation of any of the crack types in Fig. 9 have any link to dwell or interface defeat (Hauver et al., 2005)? Reverse ballistic testing of Borofloat® was conducted and its results may shed some insights into that possible link.

Experiments were conducted at Ernst-Mach-Institut (EMI) under subcontract to Southwest Research Institute (SwRI). In the experiments, a copper buffer was placed over a cylinder of Borofloat® glass. The sample was 60-mm long and 21 mm in diameter. It was launched at a stationary gold rod 1 mm in diameter and 70-mm long (i.e., a reverse ballistics experiment). Gold was used to minimize strength effects of the rod. The copper buffer was sized through numerical simulations (Holmquist et al., 2005). The cylindrically shaped copper buffer was 2.5-mm high with a diameter of 4 to 5 mm. The purpose

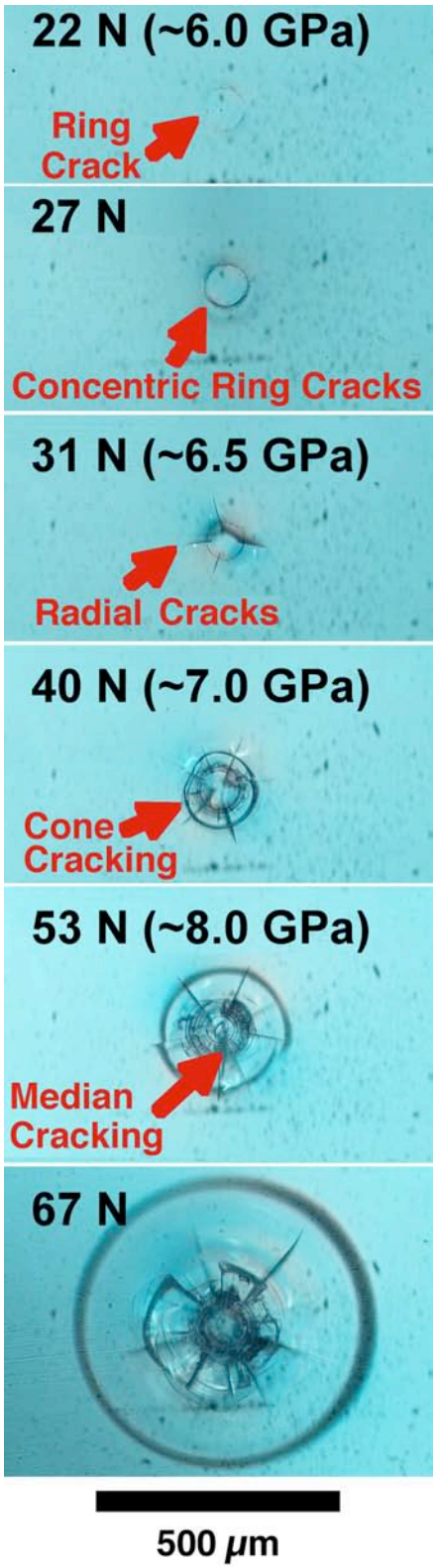

Figure 9. Sequence of crack type formation with increasing indentation load with a 300-μm-diameter indenter. Shown stress values represent an idealized Hertzian (elastic) condition.

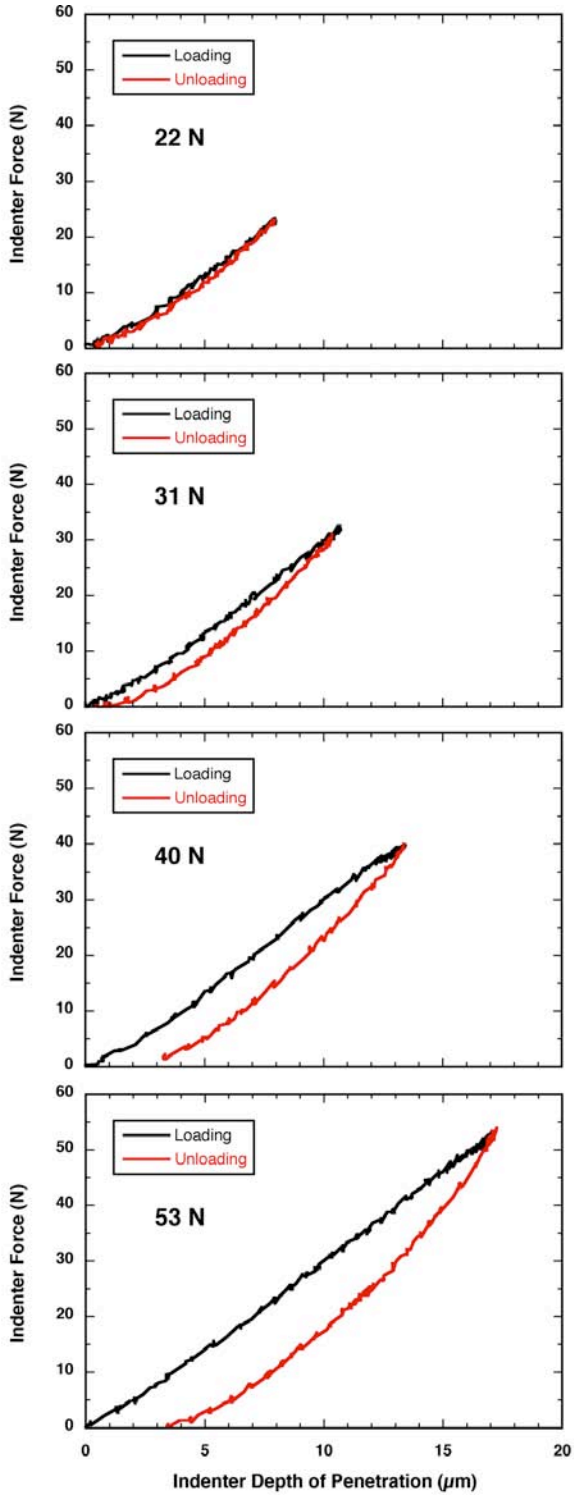

Figure 10. Indentation load/unload histories for four different maximum loads. These graphs correspond to four of the six indents shown in Fig. 8. Hysteresis starts when radial cracks form (31 N) and then it increases at a faster rate with cone (40 N) and median cracking (53 N).

of the buffer was to attenuate the impact shock. Additionally, the presence of the buffer results in "ramp" loading of the glass; and recently, there are indications that ramp loading is as important for "survival" of the glass as is attenuating the impact shock. A flash radiograph 62.4 μs after impact is shown in Fig. 11. The copper buffer and the rod are denoted in the figure. The objects on the left-hand-side of the figure are part of the sabot package used to launch the glass cylinder. Rod debris is seen flowing radially along the impact surface. The gold rod was totally defeated at the front surface of the glass. Optical pictures show that dwell existed all the way to 82.7 μs, at which time the rod had completely eroded (assuming steady-state flow, the rod should have been consumed by approximately 79 μs; therefore, the optical picture at 82.7 μs was after complete erosion).

The Bernoulli pressure (P) of the rod onto the glass is given by $P = \frac{1}{2} \bullet \rho_{gold} \bullet V^2$, where ρ_{gold} is the density of the gold and V is impact velocity. This results in a pressure of 7.6 GPa at the 890-m/s-impact velocity. If the ultimate strength of the gold rod is included in the Bernoulli stress (0.2 GPa), that increases the pressure that at the glass interface to approximately 7.8 GPa. This value is very close to the Hugoniot elastic limit observed for this material (Hill and Chhabildas, 2006). Because the rod transitioned from dwell to penetration for some impact velocities slightly lower than 890 m/s, it is conjectured that 890 m/s is near the upper limit for sustained dwell.

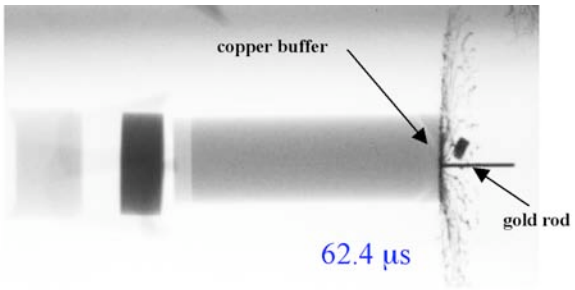

Figure 11. Flash radiograph of experiment showing interface defeat of gold rod onto Borofloat® glass (with copper buffer) at an impact velocity of 890 m/s.

The applied stress values for the spherical indents and the various damage mechanisms shown in Fig. 9 are in the vicinity of the dwell pressure measured with this reverse ballistic test. However, further scrutiny of this translation is of course needed and will be pursued in future work. The shown stress values in Fig. 9 represent idealized average Hertzian elastic stresses for the shown compressive forces. Once damage is initiated (at 22 N), the ability to estimate that average stress becomes uncertain.

3.4 Constructed Design/Damage Maps

Using the data generated and discussed in Sections 3.1 and 3.2, a Design/Damage Map was constructed for the loading scenario illustrated in Fig. 12. It consisted of a ball-on-ring setup where the ball has a 6.35-mm diameter WC ball and the support ring has a 75-mm diameter.

The relationships linking different ball sizes and different ball materials can be found in the classical literature (Johnson, 1985). A 500-µm-diameter diamond indenter was used to generate the data in Fig. 8, and those results were used to predict the contact damage response when a 6.35 mm diameter WC ball was instead used with the four conditions explored in this study.

Thicknesses between 2 and 10 mm were considered for this prediction. This thickness range was chosen because classical beam bending was maintained and the strength input from Section 3.1 would be adaptable. The effective area of the Weibull strength distributions were strength-size-scaled between the loading scenarios of Figs. 1 and 12 using established practices described elsewhere (ASTM C XXXX, 2006; Wereszczak et al., 1999; and Wachtman, 1996).

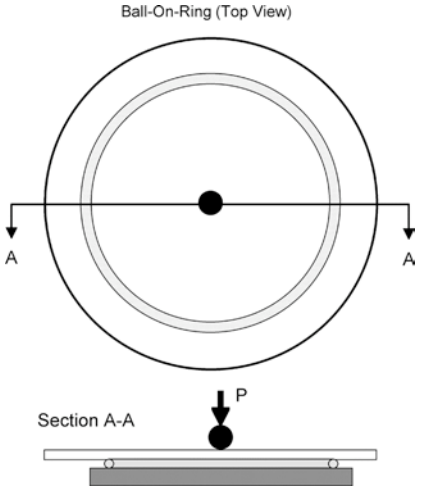

Figure 12. A Design/Damage Map was constructed for the condition when a 6.35-mm WC ball was loaded against different thicknesses of Borofloat® and Starphire®. Air and tin side orientations were considered. The glass was set on a 75-mm diameter ring.

The resulting Design/Damage maps are illustrated in Fig. 13 for the four investigated conditions. Starphire® could withstand higher forces for thicknesses less than ~ 5 mm, whereas Borofloat® could withstand higher, damage-free contact forces for thicknesses greater than ~ 6.5 mm. The maps also show that it is advantageous to orient the tin side to be the contact side *independent of the thickness for both glasses*.

This study suggests that improved ballistic performance of "float-glasses" can be achieved through appropriate selection of glass based on the thickness and the appropriate orientations of their air and tin sides if strength and indentation responses are translatable to ballistic performance. Additional attempts to link results from this suite of spherical indentation to threshold velocity and dwell pressures are already underway with other materials.

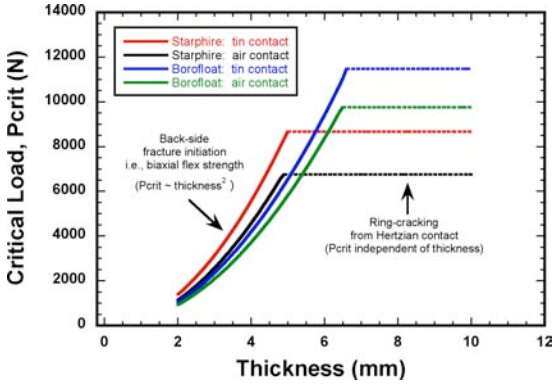

Figure 13. Design/Damage Map of the conditions described in Fig. 12. As an example to illustrate its usage, if a 7-mm-thick glass was loaded to 9000 N, then Borofloat® would not be damaged whereas Starphire® would exhibit ring cracking.

CONCLUSIONS

The flexure strength of Starphire® soda-lime glass was greater than that of Borofloat® borosilicate glass, and the air side of both was stronger than their tin side. For the same thickness of glass, this means that Starphire® glass can withstand larger flexure loads than Borofloat® glass, and both glasses can withstand higher flexure loads if their tin sides are oriented to be the impact side (i.e., the air side being the back face side). The trends were reversed for critical loads that initiated ring cracking. The Borofloat® glass was able to withstand higher, damage-free contact forces than the Starphire® glass and the tin side of both glasses could withstand higher, damage-free contact forces than their air sides. *Therefore, the trends of flexure strength and indentation responses can be beneficially exploited if the tin and air sides are oriented to be the contact and back face sides, respectively.*

Design/Damage maps were constructed to combine the flexure strength and ring-crack responses and to aid in interpretations of glass thickness dependencies. These maps showed that Starphire® glass could withstand higher flexure-induced forces for smaller thicknesses of

glass and that Borofloat® could withstand higher, damage-free contact forces for larger thicknesses. The maps also show that it is advantageous to orient the tin side to be the contact side independent of the thickness for both glasses.

If strength and indentation responses are translatable to ballistic performance, then this study shows that improved ballistic performance of "float-glasses" can be achieved through appropriate selection of glass based on thickness and appropriate orientations of their air and tin sides. Ballistic tests are now under consideration to determine if the conclusions from this study translate to improved ballistic performance.

ACKNOWLEDGMENTS

The authors wish to thank USARL's K. Iyer and J. Swab and ORNL's C. -H. Hsueh for their helpful comments and suggestions.

Research sponsored by WFO sponsor US Army Tank-Automotive Research, Development and Engineering Center under contract DE-AC05-00OR22725 with UT-Battelle, LLC.

REFERENCES

ASTM C1499, 2005a: Standard Test Method for Monotonic Equibiaxial Flexure Strength of Advanced Ceramics at Ambient Temperatures, Vol. 15.01, ASTM International, West Conshohocken, PA.

ASTM C1239, 2005b: Standard Practice for Reporting Uniaxial Strength Data and Estimating Weibull Distribution Parameters for Advanced Ceramics, Vol. 15.01, ASTM International, West Conshohocken, PA.

ASTM C XXXX, 2006: Proposed Standard Practice for Size Scaling of Tensile Strengths Using Weibull Statistics for Advanced Ceramics, ASTM International, West Conshohocken, PA.

Cook, R. F. and Pharr, G. M., 1990: Direct Observation and Analysis of Indentation Cracking in Glasses and Ceramics, *J. Am. Ceram. Soc.*, **73**, 787-817.

Hauver, G. E., Rapacki, Jr., E. J., Netherwood, P. H., and Benck, R. F., 2005: Interface Defeat of Long-Rod Projectiles by Ceramic Armor, ARL-TR-3590.

Hill, S. and Chhabildas, L. C., 2006: Sandia National Laboratories, private communication.

Holmquist, T. J., Anderson, Jr., C. E., and Behner, T., 2005: Design, Analysis and Testing of an Unconfined Ceramic Target to Induce Dwell, *Proc. 22nd Int. Symp. on Ballistics*, **2**, 860-868, DES*tech* Publications, Inc., Lancaster, PA.

Johnson, K. L., 1985: *Contact Mechanics*, Cambridge University Press, London, UK.

Lardner, T. J., Ritter, J. E., and Zhu, G. -Q., 1997: Spherical Indentation and Fracture of Glass Plates, *J. Am. Ceram. Soc.*, **80**, 1851-1862.

Lawn, B. R., 1998: Indentation of Ceramics with Spheres: A Century after Hertz, *J. Am. Ceram. Soc.*, **81**, 1977-1994.

Pavelchek, E. K. and Doremus, R. H., 1976: Static Fatigue in Glass - A Reappraisal, *J. Non-Cryst. Sol.*, **20**, 305-321.

Rhee, Y. -W., Kim, H. -W., Deng, Y., and Lawn, B. R., 2001: Contact-induced Damage in Ceramic Coatings on Compliant Substrates: Fracture Mechanics and Design, *J. Am. Ceram. Soc.*, **84**, 1066-1072.

Sands, J. M., Patel, P. J., Dehmer, P. G., and Hsieh, A. J., 2004: Protecting the Future Force: Transparent Materials Safeguard the Army's Vision, *AMTIAC Quarterly*, **8**, No. 4, 28-36.

Swain, M. V. and Hagen, J. T., 1976: Indentation Plasticity and the Ensuing Fracture of Glass, *J. Phys. D: Appl. Phys*., 9, 2201-2214.

Tillet, J. P. A., 1956: Fracture of Glass by Spherical Indenters, *Proc. Phys. Soc. London*, **B69**, 47-54.

Wereszczak, A. A., Kirkland, T. P., Breder, K. Lin, H. -T., and Andrews, M. J., 1999: Biaxial Strength, Strength-Size-Scaling, and Fatigue Resistance of Alumina and Aluminum Nitride Substrates, *Int. J. Microcircuits & Elect. Pack.*, **22**, 446-458.

Wereszczak, A. A. and Johanns, K. E., 2006a: Spherical Indentation of SiC, *Ceram. Engrg. Sci. Proc.*, in press.

Wereszczak, A. A., 2006b: Elastic Property Determination of WC Spheres and Estimation of Compressive Loads and Impact Velocities that Initiate Their Yielding and Cracking, *Ceram. Engrg. Sci. Proc.*, in press.

Wereszczak, A. A., 2006c: Determination of Elastic Properties of a WC Core Using Resonant Ultrasound Spectroscopy and Model Analysis, *RDECOM-TACOM Technical Report*, in press.

Wachtman, Jr., J. B., 1996: *Mechanical Properties of Ceramics*, John Wiley & Sons, Inc., New York, NY.